

Computational Investigation of SCL Sheath with two Dust Species

Hashmi Sayed Taha¹, Dr. Puranaik Shankar Naik²

¹Research Scholar, Sunrise University, Alwar

²Professor, Sunrise University, Alwar

Article Info: Received: 22-07-2023 / Revised: 14-08-2023 / Accepted: 30-09-2023

Address for Correspondence: Hashmi Sayed Taha

Conflict of interest statement: No conflict of interest

Abstract

There have been extensive analytical and computational investigations of plasma instabilities to comprehend potential processes for solely rising magnetic fields in the presence of mobile/immobile ions and (or) cold/mildly heated electron beams. Through the integration of kinetic, fluid, and magnetohydrodynamic (MHD) techniques, a theory has been constructed to correctly explain both rapid and slow processes in plasmas. Inertial confinement fusion, Gamma-ray bursts (GRBs), and the magnetospheres of pulsars are all offered as examples of specific applications. New and pure growth modes in quantum-plasmas, a fast-developing emergent domain of plasma physics, have also been the subject of our research. We have examined an oscillatory instability involving dust acoustic-like waves owing to a relative drift between the ions and the charged dust particles in quantum dusty magneto-plasma. Due to their presence in the plasma, nano-dusts modify the sheath dynamics by influencing the Poisson equation, which establishes the sheath plasma potential.

Keywords SCL Sheet, MHD, Dust Species, plasma

Introduction

When studying and analyzing magnetic nozzles, the collisional state of the electrons and ions is essential for determining the normal plasma behavior. The sonic and magnetic cusp speeds in the magnetic field throat have been studied experimentally and numerically to determine the limiting condition of fully collisional plasma in (high-beta) flow from a theta pinch. The results show that plasma from a static source can expand to the point of detachment from the field lines. Longmier et al. found that examining magnetic nozzle effects in the VASIMR VX-200i with Ar propellant causes plasma acceleration (to $Ma > 3$). Local axial ion speeds upstream of the magnetic nozzle have been observed to reach Mach 4, and it has been shown that an ambipolar electric field acted as the ion acceleration mechanism. At NASA's Marshall Space Flight Center, Deline et al. used a plasma cannon, magnetic nozzle coils, and RF interferometer measurements to investigate the

downstream plasma detachment process. The flow was initially low-beta along the magnetic field, but detachment occurred when the plasma kinetic pressure approached magnetic pressure levels, and a rising high-beta plume was seen as a result.

However, the 'collective conduct' of plasma is one of the most crucial needs since it distinguishes plasma from the gaseous state. It clarifies the possible spread of disturbances from a localized region to a more distant region of the plasma. In 1952 (Pines and Bohm, 1952), David Pines and David Bohm were the first to suggest that plasma shows collective behavior. Furthermore, plasma's neutrality is one of its defining characteristics. A gas that is just partially ionized is not considered plasma until it achieves a neutral state and begins to behave as a group. Latin etymology for the word "quasi" hints at a "as if" or "resembling" connotation. A neutral charge density is

achieved when a plasma achieves a condition of equilibrium. As a result of the mobility of charged particles in a plasma system, weak electric fields may be generated at smaller scales, despite the fact that the overall charge density of the system is neutral.

Literature Review

O. Larroche (2021) Hydrodynamic modeling algorithms based on the Euler equations have their limitations when it comes to describing the collisional nature of the inner plasma in various inertial confinement fusion hohlraum designs, especially at the convergence of the expanding plasma flow. To better tackle such circumstance, this research proposes an enhanced hydrodynamics model featuring higher moments of the particle velocity distribution function, combined with physically supported closure assumptions and relaxation terms. In a test example involving the collision of two plasma flows at high velocities, a preliminary one-dimensional numerical implementation of the model is demonstrated to yield good results. We briefly address potential ways to increase the dimensionality of that model to get the true hohlraum geometry.

Florian Effenberg (2019) Radiative power exhaust by impurity seeding was demonstrated for the first time in island divertor configurations at the stellarator Wendelstein 7-X. Feasibility of stable plasma operation was shown during seeding with both neon (Ne) and nitrogen (N₂). High radiative power losses (80%) were found to reduce the divertor heat loads globally by 2/3 with both seeding gases injected at a single toroidal location into one of five magnetic islands. Heat flux detachment was achieved for the price of a loss of (%) in the stored energy. Ne seeding allows for sustained enhancement of edge radiation with a very slow decay of line emission of several tens of seconds after the end of the injection indicating a high recycling of this noble gas at the carbon main plasma facing components. In N₂ seeded discharges it is shown that a response of line emission and plasma parameters is in correlation to the puff duration which indicates a higher level of absorption of this seeding gas in the wall. Continuous N₂ seeding results in global cooling of the scrape-

off layer (SOL) and decay of radiation over several seconds after the injection. Damping of counter-streaming SOL flows, and divertor particle fluxes induced by Ne and N₂ seeding have been measured and provide evidence for a reduction of the convective part of the divertor heat fluxes. Losses in density in response to seeding can be compensated by feedback controlled divertor fueling. The controlled reduction of heat fluxes within this complex 3D edge island geometry is a very promising finding concerning detachment control in a future all-metal divertor.

Dieter Boeyaert (2021) The ability of future tokamaks to dissipate energy near the plasma's edge is crucial. High confinement mode (H-mode) EAST discharges are used to evaluate neon's viability as a radiative seeding species in a disconnected double null (DDN) arrangement. The advantages of the double null topology are diminished since the distance between the two separatrices in the analyzed DDN discharges is at most 1.5 centimeters. On the other hand, neon seeding has a beneficial effect: under high-recycling settings, both the divertor temperature and the target heat flux drop by more than a factor of five as the seeding rate rises. In order to aid in the continuing transport study, we offer SOLPS-ITER simulations of the edge plasma with an interpretive focus. Numerical findings for the unseeded scenario agree with experimental data for the desired temperature settings and observed neutral pressures in the active divertor within a factor of two. Appropriate selection of coefficients for anomalous transport and neutral conductances between the top cryopump and the main chamber is the key to establishing satisfactory agreement.

J. M. Canik et.al (2017) Major inconsistencies between experiment and modeling of dissipative divertor operation are discussed, with a focus on recent research in DIII-D helium plasmas and the involvement of atomic and molecular physics. Helium operation eliminates the intricate molecular processes of deuterium plasmas that are a major contender for the inadequacy of ordinary fluid models to recreate dissipative divertor operation, especially the constant under-prediction of radiated power. Full divertor radiation may be

accounted for in models of these studies, but only if care is made to recreate the observed divertor density. Better modeling of the link between the divertor and the upstream scrape-off layer is required since using upstream data leads to a lower divertor density and radiation than is observed. These findings demonstrate the efficacy of fluid models in describing the divertor-region plasma, including radiative losses, and suggest that attempts to increase the accuracy of the molecular deuterium models are likely to aid in resolving the disparity in radiation for deuterium plasmas.

Lauren N. Woolsey (2016) Since the 1950s, scientists have known that the Sun emits a constant, supersonic outflow that we call the solar wind, and that the acceleration of the wind is directly related to the presence of the million-degree solar corona. Unanswered questions in solar physics include what causes the wind to accelerate and how the corona heats up. In this paper, I zero down on one kind of acceleration in an effort to shed light on this conundrum. The movement of the magnetic field's footpoints in the photosphere gives rise to Alfvén waves. Magnetic loops and flux tubes that extend into the heliosphere permeate the whole corona. My research has focused on elucidating the function of these magnetic fields in setting the parameters of the solar wind in open flux tubes. After a brief context setting, I will talk about the parameters I studied in order to have a better statistical grasp of the magnetic field profiles and the associated SteadyState wind. In the next chapter, I will detail how I expanded this work to account for time dependency in the turbulent heating by Alfvén waves in 3D simulations. As a natural extension of my theoretical work, I have begun analyzing observations of small network jets in the chromosphere and transition region, as well as the underlying photospheric magnetic field that forms thresholds in jet production, due to the bursty nature of this heating. In conclusion, this study examines the breadth to which Alfvén-wave-driven turbulent heating may account for known occurrences and measured parameters of the solar wind.

The Physics of an SCL Sheath

The presence of a SCL sheath is influenced by the dynamic between the sheath region's net quantity of electrons and the ions present there. In what follows, we attempt to describe the fundamental physical processes that lead to the creation of a SCL sheath, with the presumption that the wall's emitted electrons are largely photoelectrons. For a floating wall that draws zero net current at an equilibrium condition in the plasma, the net fluxes of distinct particles at the wall are equal and opposite. This is represented by the notation j , where j specifies the species,

$$\Gamma_e = \Gamma_{pe} - \Gamma_{ph} = \Gamma_i \quad (1)$$

Where e is the difference between the plasma electron flux and the photoelectron flux at the wall, and where the net electron flux at the wall must equal the net ion flux. When there is no wall emission, the traditional situation often applies, $\Gamma_{pe} \gg \Gamma_i$, as a result of the wall's potential $\phi_w < 0$, using the zero potential assumption for the plasma bulk. This causes the incoming electrons to be reflected back off the wall, keeping the bulk plasma in a quasineutral state, $\Gamma_{pe} \approx \Gamma_i$. Now think about wall-emitted electrons, i.e. $\Gamma_{ph} > 0$. For small Γ_{ph} , since the net negative charge layer is thinner than the sheath's positive ion layer, the wall charge is still minuscule, and the potential rises monotonically from a minuscule value at the wall to the bulk plasma, where it is positive $\phi = 0$. However, when $\Gamma_{ph} \rightarrow \Gamma_{cr}$, the SCL transition happens when the electric field at the wall vanishes and the potential at the wall flattens out at a critical value. This is because the electric field at the wall is equal to the electric field at the sheath. When $\Gamma_{ph} > \Gamma_{cr}$, compared to its surroundings, the sheath's negative layer is much stronger than the sheath's positive layer, and the wall charges to a positive value. Keep in mind that because we are trying to keep the bulk plasma potential at zero, the wall potential must go from being positive at the wall to being negative as a whole with regard to the bulk plasma. Nonetheless, the SCL sheath forms as one travels away from the wall because the negative layer gets thinner than the positive layer and the potential begins to rise. Our

research focused on what happens when the wall potential becomes positive relative to the bulk plasma potential as a result of the negative charge layer forming at the wall and in the surroundings when ϕ is increased.

Mechanisms for the Plasma Magnetization

Motivation

In the past several decades, researchers have examined the creation of magnetic fields in a variety of physical contexts, from the cosmos (supernova remnants, gamma-ray bursts) to laser-produced plasmas. Magnetic fields are therefore discovered to be significant throughout the whole size hierarchy of different plasma systems. How can a non-zero "seed magnetic field" arise in a plasma with no magnetic field at all to begin with? To address this issue, we need to determine what processes produce the electron current j_e and the electric field E that are prerequisites for producing the seed magnetic field B . To simplify, we ignore the displacement current in Maxwell's equations and get at

$$\nabla \times \mathbf{B} \approx \mu_0 \mathbf{J} \equiv -\mu_0 e (n_e \mathbf{v}_e - n_i \mathbf{v}_i), \tag{2}$$

$$\frac{\partial \mathbf{B}}{\partial t} = -\nabla \times \mathbf{E}, \tag{3}$$

where the velocities of electrons and ions in their fluids v_e and v_i , in The plasma and electromagnetic wave intensity gradients, in turn, are governed by the electromagnetic fields E and B . Since electric fields and currents result from the collision of moving electrons and ions, the primary concern is on tearing the electrons and ions apart.

It has been shown that a variety of processes, such as non-parallel electron density and temperature gradients, may produce the seed magnetic fields in plasmas. $(\nabla n_e \times \nabla T_e)$ known as the Biermann battery), by the ponderomotive forces of strong laser beams, by electron temperature anisotropy (known as the Weibel instability), and by counter streaming charged particle beams (known as the current-filamentation instability, related to the inverse Faraday effect). These methods explain how currents and the space charge electric field,

which provide plasmas with their seed magnetic fields, are produced by the mobility of electrons. In the next subsections, we will go over each of these procedures for the creation of the magnetic field in more depth.

THE $\nabla n_e \times \nabla T_e$ (THE BIERMANN BATTERY)

In the context of rotating magnetized stars, Schlutter and Biermann showed approximately sixty years ago that the presence of an electron temperature gradient that is not parallel to the density gradient will result in the formation of a pressure force in a non-relativistic plasma without equilibrium electron flow $\nabla \cdot \mathbf{P}_e$, where

the pressure of electrons is $P_e = k_B n_e T_e$. It will cause a space charge electron field and electron currents by quickly pushing the lighter electrons against the heavier ions. The non-relativistic electron momentum equation is used to calculate the electric field, ignoring the linear and nonlinear inertia of the electron stream.

$$0 = -e (\mathbf{E} + \mathbf{v}_e \times \mathbf{B}) - \frac{k_B T_e \nabla n_e}{n_e} - \frac{k_B n_e \nabla T_e}{n_e}, \tag{4}$$

This demonstrates how the electron pressure gradient and electromagnetic forces cancel each other out in plasmas.

We may now remove E from (3) by using Eq. (4), yielding

$$\frac{\partial \mathbf{B}}{\partial t} = \nabla \times (\mathbf{v}_i \times \mathbf{B}) + \frac{1}{\mu_0 e n_e} \nabla \times [\mathbf{B} \times (\nabla \times \mathbf{B})] + \frac{k_B}{e n_e} (\nabla T_e \times \nabla n_e) \tag{5}$$

where we have assumed $n_i = n_e$. Eq. (6) implies that when the equilibrium electron temperature and density gradients are non-parallel, the baroclinic vector—the third component in the right-hand side of non-zero—must be non-zero. The magnetic fields in the seeds are caused by this baroclinic vector. The ion flow and the $\mathbf{j} \times \mathbf{B}$ force are connected to the first and second terms on the right side of equation (6), respectively. Their significance arises during the extended development of magnetic fields that arise naturally due to the non-parallel variations in electron temperature and density. Therefore, when there is an angle between the equilibrium density and

temperature gradients in plasmas, this process produces a dc magnetic field.

Considering the baroclinically generated magnetic fields in laser-produced plasmas

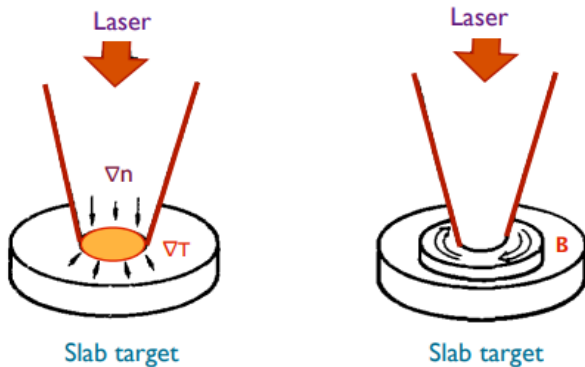


Figure 1: Schematic representation of toroidal dc magnetic fields produced by the $\nabla n_e \times \nabla T_e$ mechanism

were looked at by Stamper and associates. This technique may be simply described as follows:

This process is more likely to take place at the outside portions of the laser spot for a target that is exposed to a single, finite-sized laser beam, as seen in Fig. 1. While the temperature gradient at the edge of the laser spot points radially inward toward the axis of the laser beam, the density gradient points toward the solid-density target face. With a scale size similar to the spot radius and a toroidal form, the magnetic field has a zero value at the laser beam's axis. Radial temperature gradients are assumed to be minor around the center of the focus point since the laser beam's intensity distribution is often quite flat there. As a result, low magnetic fields are anticipated at the focus region's center. Over a period t , the magnetic field's order of magnitude is approximately $\delta t (m_e/e) (V_{Te}^2 / L_n T_T) \sin \theta$,

where $V_{Te} = (k_B T_e / m_e)^{1/2}$ is the electron thermal speed, L_n and L_T are the gradients of electron temperature and density scale lengths, respectively, and θ is the angle formed by the temperature and density inhomogeneities' directions.

One might balance the baroclinic driver and the curl of the magnetic field B_s to determine the steady-state size of the magnetic field $B_s \mathbf{u} \times \mathbf{B}$,

where $\mathbf{u} = \langle \mathbf{v}_i \rangle$ is the average ion fluid velocity outward, as determined by Eq. (5)

$$B_s \simeq \left(\frac{m_e L}{e} \right) \left(\frac{V_{Te}^2}{c_s L_n L_T} \right) \quad (6)$$

where L is the variation's scale size $\mathbf{u} \times \mathbf{B}$ flow $|\mathbf{u}| \sim c_s$, and c_s is the speed of sound ions. It is assumed that the angular factors resulting from the different cross products in Eq. (6) are of order unity.

Conclusion

Both non-relativistic and relativistic plasma outflows are common in laboratory plasmas and astrophysical settings. Return currents in the opposite direction are created when relativistic and non-relativistic charged particle beams propagate through background plasmas. Interactions between the currents subsequently cause a number of plasma instabilities, including longitudinal (electrostatic instabilities) and transverse (electromagnetic instability) modes. In order to comprehend potential processes for solely rising magnetic fields in the presence of mobile/immobile ions and/or cold/mildly heated electron beams, extensive analytical and computational investigations of plasma instabilities have been conducted. The theory has been constructed utilizing the fluid, kinetic, and magnetohydrodynamic (MHD) techniques to provide a good explanation of both rapid and slow events in plasmas. As a result, we have independently determined the SCL sheath structure and the wall-distance at which the sheath's potential is lowest. Despite the fact that the nano-dusts behave like ions in every way, they are unable to penetrate further than the minimum potential due to their modest velocities. As a result, they won't add up and influence the possible profile until after the SCL drop. When the micron-dusts enter the sheath, they start to accumulate enormous amounts of charges.

REFERENCE

1. O. Larroche "An extended hydrodynamics model for inertial confinement fusion hohlraums"2021

2. Effenberg, Florian & Brezinsek, Sebastijan & Feng, Y. & Koenig, Ralf & Krychowiak, Maciej & Jakubowski, Marcin & Niemann, Holger & Perseo, Valeria & Schmitz, Oliver & Zhang, Daihong & Barbui, Tullio & Biedermann, Christoph & Burhenn, Rainer & Buttenschön, Birger & Kocsis, G. & Pavone, Andrea & Reimold, Felix & Szepesi, Tamas & Frerichs, Heinke & Pedersen, Thomas. (2019). First Demonstration of Radiative Power Exhaust with Impurity Seeding in the Island Divertor at Wendelstein 7-X. *Nuclear Fusion*. 59. 10.1088/1741-4326/ab32c4.
3. Boeyaert, Dieter & Wiesen, S. & Wischmeier, Marco & Dekeyser, Wouter & Carli, Stefano & Wang, L. & Ding, Fang & Li, K. & Liang, Y. & Baelmans, Martine. (2021). Towards assessment of plasma edge transport in Neon seeded plasmas in disconnected double null configuration in EAST with SOLPS-ITER. *Nuclear Materials and Energy*. 26. 100926. 10.1016/j.nme.2021.100926.
4. Canik, J. & Briesemeister, A. & McLean, A. & Groth, Mathias & Leonard, A. & Lore, J.D. & Moser, A. (2017). Testing the role of molecular physics in dissipative divertor operations through helium plasmas at DIII-D. *Physics of Plasmas*. 24. 056116. 10.1063/1.4982057.
5. Lauren N. Woolsey “Magnetic Influences on the Solar Wind” May 2016
6. Zhao, Menglong & Jaervinen, A.E. & Joseph, Ilon & Rognlien, T.D. (2020). Impact of ion temperature anisotropy on 2D edge-plasma transport. *Nuclear Materials and Energy*. 26. 100881. 10.1016/j.nme.2020.100881.
7. Chicheportiche, Alexandre & Lepetit, B & Benhenni, M. & Gadéa, Florent & Yousifs, Mohammed. (2013). Comparative study of collision cross-sections and ion transport coefficients from several He⁺/He interaction potentials. *Journal of Physics B: Atomic, Molecular and Optical Physics*. 46. 065201. 10.1088/0953-4075/46/6/065201.
8. Kenneth W. Dunn et.al “A practical guide to evaluating colocalization in biological microscopy”
<https://doi.org/10.1152/ajpcell.00462.2010>
9. Chaojie Zhang et.al “Mapping the self-generated magnetic fields due to thermal Weibel instability” 2022 Vol. 119 No. 50 e2211713119
<https://doi.org/10.1073/pnas.2211713119>
10. Nishikawa, K.-I.; Mizuno, Y.; Gómez, J.L.; Duřan, I.; Meli, A.; Niemiec, J.; Kobzar, O.; Pohl, M.; Sol, H.; MacDonald, N.; et al. Relativistic Jet Simulations of the Weibel Instability in the Slab Model to Cylindrical Jets with Helical Magnetic Fields. *Galaxies* 2019, 7, 29. <https://doi.org/10.3390/galaxies7010029>
11. Rouillard, Alexis & Viall, N. & Pierrard, Viviane & Vocks, Christian & Matteini, Lorenzo & Alexandrova, O. & Higginson, Aleida & Lavraud, Benoit & Lavarra, Michael & Wu, Yihong & Pinto, Rui & Bemporad, Alessandro & Sanchez-Diaz, Eduardo. (2021). The Solar Wind. 10.1002/9781119815600.ch1.
12. Matteini, L. & Franci, Luca & Alexandrova, O. & Lacombe, Catherine & Landi, Simone & Hellinger, P. & Papini, Emanuele & Verdini, A.. (2020). Magnetic Field Turbulence in the Solar Wind at Sub-ion Scales: In Situ Observations and Numerical Simulations. *Frontiers in Astronomy and Space Sciences*. 7. 10.3389/fspas.2020.563075.
13. Kajdič, P. & Alexandrova, O. & Maksimovic, M. & Lacombe, Catherine & Fazakerley, A.. (2017). Suprathermal Electron Strahl Widths In The Presence Of Narrow-Band Whistler Waves In The Solar Wind. *The Astrophysical Journal*. 833. 10.3847/1538-4357/833/2/172.
14. Lacombe, Catherine & Alexandrova, O. & Matteini, Lorenzo. (2017). Anisotropies of the Magnetic Field Fluctuations at Kinetic Scales in the Solar Wind: Cluster Observations. *The Astrophysical Journal*. 848. 10.3847/1538-4357/aa8c06.
15. Zenteno-Quinteros, Bea & Moya, Pablo & Lazar, Marian & Viñas, Adolfo & Poedts, Stefaan. (2023). Interplay between Anisotropy- and Skewness-driven Whistler Instabilities in the Solar Wind under the Core–Strahl Model. *The Astrophysical Journal*. 954. 184. 10.3847/1538-4357/ace973.